Impacts of Horizontal Propagation of Orographic Gravity Waves on the Wave Drag in the Stratosphere and Lower Mesosphere

Xin Xu[1], Yuan Wang[1*], Ming Xue[1,2], and Kefeng Zhu[1]

[1]Key Laboratory of Mesoscale Severe Weather/Ministry of Education, School of Atmospheric Sciences, Nanjing University, Nanjing, Jiangsu, China

[2]Center for Analysis and Prediction of Storms, University of Oklahoma, Norman, OK, USA

Corresponding author: Yuan Wang (yuanasm@nju.edu.cn)

Key Points:

- Impact of horizontal propagation of mountain wave on wave drag in the stratosphere and lower mesosphere is evaluated using reanalysis data.
- Horizontal propagation reduces (enhances) the orographic wave drag in the lower stratosphere (mid-upper stratosphere and lower mesosphere).
- The impact of horizontal propagation is most prominent in winter, over the western Tibetan Plateau, Rocky Mountains, and Greenland.
- Incorporation of horizontal propagation in orographic wave drag parameterization can potentially alleviate commonly seen model wind and temperature biases.

Abstract

The impact of horizontal propagation of mountain waves on the orographic gravity wave drag (OGWD) in the stratosphere and lower mesosphere of Northern Hemisphere is evaluated for the first time. Using a fine-resolution (1-arc minute) terrain and 2.5°×2.5° ECMWF ERA-interim reanalysis data during 2011-2016, two sets of OGWD are calculated offline according to a traditional parameterization scheme (without horizontal propagation) and a newly proposed scheme (with horizontal propagation). In both cases, the zonal-mean OGWD show similar spatial patterns and undergo a notable seasonal variation. In winter, the OGWD is mainly distributed in the upper stratosphere and lower mesosphere of mid-high latitudes, whereas the summertime OGWD is confined in the lower stratosphere. Comparison between the two sets of OGWD reveal that the horizontal propagation of mountain waves tends to decrease (increase) the OGWD in the lower stratosphere (mid-upper stratosphere and lower mesosphere). Consequently, including the horizontal propagation of mountain waves in the parameterization of OGWD can reduce the excessive OGWD in the lower stratosphere and strengthen the insufficient gravity wave forcing in the mesosphere, which are the known problems of traditional OGWD schemes. The impact of horizontal propagation is more prominent in winter than in summer, with the OGWD in western Tibetan Plateau, Rocky Mountains and Greenland notably affected.

1 Introduction

Most mountain waves, or orographic gravity waves (OGWs), are unresolved subgrid-scale phenomena in general circulation models (GCMs) and chemistry climate models (CCMs). In spite of their small horizontal scales, these waves are of great importance in transporting the momentum and energy from the lower troposphere to the middle atmosphere. The breaking of mountain waves produces a body force known as orographic gravity wave drag (OGWD), which has been shown to play an vital role in shaping the general circulation in the middle atmosphere [e.g., *Holton*, 1983; *Fritts and Alexander*, 2003; *McLandress and Shepherd*, 2009] as well as in the troposphere through the downward control mechanism [*Haynes et al*., 1991]. In order to reproduce a realistic atmospheric circulation, the effects of OGWD need to be accounted for in climate models.

First developed in early 1980s, the parameterization of OGWD is implemented in nearly all modern global models [e.g., *Lott and Miller*, 1997; *Scinocca and McFarlane*, 2000; *Kim and Doyle*, 2005]. With the aid of OGWD parameterization, the performance of global models has been improved substantially [e.g., *Palmer et al*., 1986]. However, current GCMs/CCMs still suffer from systematic temperature and wind biases that might be attributed to inadequate parameterization of OGWD. For instance, climate models often produce an unrealistic upright northern polar-night jet. The lack of vertical tilt of the jet in turn yields a weak meridional gradient of temperature in the polar mesosphere through the thermal wind balance[*Kim*, 2007]. The simulated polar vortex in the lower stratosphere of Southern Hemisphere is often too cold as compared to observations [*McLandress et al*., 2012]. This cold-pole bias results in unrealistic ozone depletion in Antarctica, which notably affects the simulated climate of Southern Hemisphere [*Polvani et al*., 2011]. *Long et al*. [2012] validated the accuracy of the British Met

Office middle atmospheric analyses against satellite observations. Considerable temperature biases (i.e., a few tens of K) were revealed in the mesosphere, implying insufficient gravity wave forcing there. Therefore, improving the parameterization of OGWD in climate models remains an important issue.

Efforts are being made to more accurately represent the OGWD in GCMs/CCMs. *Choi and Hong* [2015] updated the subgrid-scale orographic parameterization by including the effects of terrain anisotropy and flow blocking drag, which contributed positively to the short- and medium-range forecasts of the Global/Regional Integrated Model system (GRIMs) global model program (GMP). The seasonal simulation was also improved throughout the troposphere and stratosphere during boreal winter. *Garcia et al.* [2017] modified the parameterization of OGWD in the Whole Atmosphere Community Climate Model (WACCM) by removing the “land fraction” factor and explicitly considering the low-level wind orientation with respect to the topography. With this updated scheme, the structure of simulated Antarctic polar vortex was improved; the long-term trend of temperature in the polar cap of Southern Hemisphere was better captured as well [*Calvo et al*., 2017].

Given the complexity of realistic mountain waves (e.g., their generation and propagation), there are still formidable challenges in representing the OGWD in climate models. Specifically, traditional OGWD parameterization schemes assume that mountain waves only propagate vertically within the model grid column where they are triggered. However, satellite observations revealed that mountain waves can propagate horizontally as far as several hundreds of kilometers away from their source region [e.g., *Alexander et al*., 2009; *Alexander and Teitelbaum*, 2011; *Jiang et al*., 2014], even for hydrostatic mountain waves [e.g., *Smith*, 1980]. Owing to the horizontal propagation of mountain waves, the local wave amplitude will be reduced with height, which in turn affects the breaking of mountain waves [*Eckermann et al*., 2015; *Xu et al*., 2017]. As studied in *Broutman et al*. [2017] for orographic gravity waves triggered by the Auckland Island, this effect can even dominate those of refraction and background density variation and thus cannot be neglected in the parameterization of OGWD.

The horizontal propagation of mountain waves is so far not taken into account in any operational OGWD scheme, as far as we know. Based on the Gaussian beam approximation (GBA) [*Pulido and Rodas*, 2011], *Xu et al*. [2017] proposed a new OGWD parameterization scheme involving the horizontal propagation of mountain waves. Unlike the standard ray theory, the GBA is a higher-order ray approximation. For a given ray tube, it takes into account not only the contribution of this ray but also a beam of rays around it. Consequently, the ray solution can be well defined even at caustics where multiple rays intersect [*Pulido and Rodas*, 2011]. In this work, the impact of horizontal propagation on the OGWD is evaluated for the first time using the GBA-based scheme as well as a traditional scheme that does not consider the horizontal propagation. Particular attention is paid to the OGWD in the stratosphere and lower mesosphere (between z = 10 km and 55 km) of Northern Hemisphere, since the tropics and Southern Hemisphere are predominantly covered by the ocean.

The rest of this paper is organized as follows. Section 2 briefly describes the dataset and methodology. Section 3 presents and compares two sets of OGWD calculated from two different parameterization schemes. Finally, this paper is summarized in section 4.

2 Dataset and methodology

In theory, breaking mountain waves can exert a body force (i.e., OGWD) on the mean flow through the deposition of gravity wave momentum, i.e.,

$$\mathbf{F}_{GW} = \frac{\partial \overline{\mathbf{v}}}{\partial t} = \frac{1}{\bar{\rho}(z)}\frac{\partial \boldsymbol{\tau}}{\partial z} = \frac{1}{\bar{\rho}(z)}\frac{\partial}{\partial z}\left[-\bar{\rho}(z)\overline{\mathbf{v}'w'}\right], \quad (1)$$

where $\bar{\rho}(z)$ is the base-state density, $\overline{\mathbf{v}}$ is the mean-flow horizontal velocity, and $\mathbf{v}'$ and w' are the wave-induced horizontal and vertical velocity perturbations. Obviously, the OGWD is closely related to the vertical distribution of wave momentum flux (WMF), i.e., $\overline{\mathbf{v}'w'}$. The nature of OGWD parameterization is to represent the WMF by unresolved topography and resolved large-scale flow properties (e.g., wind and temperature).

In this work, the daily, 2.5°×2.5° ERA-interim reanalysis data in the period of 2011-2016 is adopted to provide the background fields (*U*, *V* and *T*) for mountain waves. Produced at the European Centre for Medium-Range Weather Forecasts (ECMWF) [*Dee et al.*, 2011], this dataset has 60 levels in the vertical, with the model top located at 0.1 hPa (i.e., in the lower mesosphere). For the subgrid-scale orography (SSO), the 1-arc-minute Global Relief Model (ETOPP1) is employed, which is developed at National Centers for Environmental Information (NCEI) of NOAA [*Amante and Eakins*, 2009]. Figure 1a displays the main topography on the Northern Hemisphere (north of 15°N), which includes the Tibetan Plateau, Mongolian Plateau and Iranian Plateau in Asia, the Rocky Mountains along the western coast of North America, and Greenland in high latitudes, etc. The topographic forcing within the grid cell of the 2.5°×2.5° ERA-interim reanalysis can be measured by the standard deviation (SD) of SSO inside the cell. As shown in Fig. 1b, the SSO SD is in general less than 400 m, with moderately high SD located over the Iranian Plateau, southern Rocky Mountains, and Greenland. Large SDs in excess of 1000 m are mainly located over the western Tibetan Plateau.

According to the 1-arc-minute SSO and 2.5° ECMWF ERA-Interim reanalysis, two sets of OGWD are calculated *offline*. For the first set, we use the parameterization scheme employed by the ECMWF forecast model [*Lott and Miller* 1997, hereafter LM97]. The other set uses the newly proposed parameterization scheme in *Xu et al*. [2017, hereafter X17]. Consistent with the LM97 scheme, mountain waves in the GBA-based scheme are assumed to be hydrostatic and irrotational, with the vertical wavenumber give by

$$m(z)^2 = \frac{N^2 K^2}{(Uk+Vl)^2}\left[1 - (Uk + Vl)\left(k\frac{\partial^2 U}{\partial z^2} + l\frac{\partial^2 V}{\partial z^2}\right)\right], \quad (2)$$

where N is the Brunt-Väisälä frequency, K is the horizontal wave number $\mathbf{K} = (k, l)$ magnitude, and $\mathbf{V}(z) = (U(z), V(z))$ is the horizontally homogeneous mean wind. The second term within the square bracket of Eq. (2) denotes the effect of wind vertical curvature. According to *Teixeria et al*. [2004] and X17, this effect has a large influence only at low Richardson number (Ri) of order unity. For the realistic atmospheric conditions, the Richardson number is usually greater than 10 such that it is omitted herein.

In order to facilitate the comparison, mountain waves in the two schemes are launched from the same reference level with equal WMF. The reference level is jointly determined by the SD of SSO and the low-level mean wind and stratification [see LM97]. Below the reference level the airflow is blocked and forced to go around the topography [e.g., *Miranda and James*, 1992]. Flow blocking can produce a form drag which is usually a substantial part of the subgrid surface stress [e.g., *Sandu et al*., 2015]. However, this drag is not considered in the present study since we are only interested in freely propagating mountain waves. Indeed, the form drag is treated independently of the OGWD in the model (see LM97). Therefore, neglecting the form drag would not influence the OGWD examined herein. The WMF at the reference level is calculated according to the GBA solution [see X17]. Specifically, the wavefield is constructed through the superposition of 20×20 Gaussians, with a spectral resolution of $2\pi/2.5°$ (which is thus latitude-dependent). The relatively small amount of Gaussians is due to that the GBA solution involves integral of the vertical wavenumber (see Eq. (4) in X17) which is time consuming. The WMF is then progressed upward level by level. At each level, the maximum wave amplitude is compared with the saturation wave amplitude (see Eq. (23) in X17), which is derived using $Ri < 0.25$ for the onset of dynamic instability [*Palmer et al*., 1986]. If the local wave amplitude exceeds the saturation wave amplitude, the waves will break and deposit the momentum into the mean flow, leading to a vertical divergence of the WMF (i.e., OGWD). Otherwise, the WMF is unchanged and passed to the next level. This differs a little bit from the parameterization scheme proposed in X17——the horizontal propagation of mountain waves may cause leakage of waves from the model grid column where they are excited, such that the WMF associated with the leaked waves are neglected when calculating the OGWD. As in this work, this portion of WMF is retained (i.e., the WMF is constant with height in the absence of dissipation), because the horizontal spread of mountain waves would not necessarily cause wave breaking and hence vertical divergence of the WMF.

3. Results

For simplicity, the OGWD obtained from the LM97 scheme is termed OGWD_V since mountain waves only propagate *vertically* in this scheme. The X17 scheme additionally includes the *horizontal* propagation of mountain waves such that the corresponding OGWD is termed

OGWD_H. The difference between the two sets of OGWD is OGWD_D, defined as OGWD_H minus OGWD_V.

3.1 OGWD_V

Figure 2 displays the zonal-mean OGWD_V in the stratosphere and lower mesosphere of Northern Hemisphere averaged during 2011-2016. In winter (December, January and February), the mountain wave drag in mid-lower latitudes (20°N~45°N) mainly occurs in the lower stratosphere between z = 15 and 20 km (Fig. 2a). In contrast, widespread drag is observed in the mid-upper stratosphere and lower mesosphere (above z = 30 km) of median high latitudes (50°N~75°N). This is qualitatively consistent with the numerical simulation of *Kim* [2007] using the Navy Operational Global Atmospheric Prediction System (NOGAPS) extended to the middle atmosphere. In high latitudes, the OGWD_V appears to increase with height, presumably owing to the decay of atmospheric density with height (see Eq. (1)). In summer (June, July and August), the OGWD_V almost vanishes south of 30°N except near the stratopause (Fig. 2c). Conversely, the mountain wave drag north of 30°N is confined in the lower stratosphere below z = 20 km. A local drag maximum is present between 45°N and 50°N around z = 17 km. Then the drag increases poleward from about 60°N, peaking at a lower altitude of about z = 12.5 km. For the OGWD_V in spring (March, April and May) and autumn (September, October and November), they are quite similar to that in winter (Figs. 2b and 2d), representing the transition between winter and summer.

Figure 3 shows the geographical distribution of OGWD_V in the mid-lower stratosphere (averaged between z = 10 and 25 km) and upper stratosphere and lower mesosphere (averaged between z = 40 and 55 km) respectively. In winter, the mid-lower stratospheric OGWD_V basically occurs over the Tibetan Plateau and central Rocky Mountains (Fig. 3a). Remarkable mountain wave drag is also observed in Greenland and Japan. In the upper stratosphere and lower mesosphere (Fig. 3b), the drag is decreased in the lower latitudes (e.g., southern Rocky Mountains, southern China) as well as in Japan. By contrast, the OGWD_V is amplified in mid-high latitudes, especially in northern Rocky Mountains, Mongolian Plateau, and Greenland. In summer, the OGWD_V is distributed in much smaller regions than in winter. In the mid-lower stratosphere, the mountain wave drag is largely located over the central Rocky Mountains, Mongolian Plateau, and Greenland (Fig. 3c); in the upper stratosphere and lower mesosphere, however, the drag disappears north of 30°N, only occurring in the lower latitudes (Fig. 3d).

3.2 OGWD_H

Figure 4 is similar to Fig. 2 but presents the zonal-mean OGWD_H in the stratosphere and lower mesosphere of Northern Hemisphere averaged during 2011-2016. The overall patterns of zonal-mean OGWD_H in the four seasons are in broad agreement with those of OGWD_V. In winter (Fig. 4a), notable OGWD_H is observed in the lower stratosphere of mid-lower latitudes but at slightly higher altitudes than OGWD_V. Moreover, there is another drag center located in the upper stratosphere near z = 40 km. In mid-high latitudes, the OGWD_H is predominantly distributed in the upper stratosphere and lower mesosphere, which is consistent with OGWD_V. In the summertime (Fig. 4c), the zonal-mean OGWD_H is confined beneath z = 25 km between 30°N and 55°N, whereas the drag north of 60°N extends up to z = 45 km, much higher than that of OGWD_V. In the lower latitudes, the OGWD_H is observed in the upper stratosphere and lower mesosphere as in the case of OGWD_V, but with larger vertical and horizontal extensions. For the geographical distribution of OGWD_H, it is of similar patterns to that of OGWD_V (not shown).

Nonetheless, there are still differences between the two sets of OGWD. As shown in Fig. 5, the X17 scheme tends to produce smaller OGWD in the lower stratosphere than the LM97 scheme; on the contrary, the mountain wave drag in the mid-upper stratosphere and lower mesosphere is enhanced, especially in winter. In consequence, the difference in the mid-lower stratosphere (below about z = 25 km) exhibits a dipole pattern. Figure 6 further displays the geographical distribution of OGWD_D at different levels. Taking the winter season as an example, OGWD_H is smaller than OGWD_V in most of mid-lower latitudes between z = 16~18 km (Fig. 6a). Salient differences are found over the western Tibetan Plateau and southern Rocky Mountains. Moving a few kilometers aloft (Fig. 6b), the OGWD_H exceeds the OGWD_V in nearly all the Northern Hemisphere. As in the upper stratosphere and lower mesosphere (Fig. 6c), there is also widespread enhancement of OGWD_H, especially in mid-high latitudes, e.g., the northern Rocky Mountains and Greenland. The spatial distribution of summertime OGWD_D is similar to its winter counterpart but with relatively small magnitude.

3.3 Discussion

According to the above analyses, the OGWD in the stratosphere and lower mesosphere of Northern Hemisphere experiences a seasonal cycle. Given the invariant topographic forcing, this seasonal variation is definitely attributed to the different circulation patterns in the four seasons. Figure 7 illustrates the zonal-mean background wind (i.e., the horizontal wind of the 2.5° ERA-interim reanalysis) between the upper troposphere and lower mesosphere of Northern Hemisphere averaged during 2011-2016. It is noteworthy that neither of the two OGWD parameterization schemes takes into account the direction change of background wind with height, namely, the background wind is *unidirectional*. It is *the wind along the direction of low-level mean wind* (see LM97) that is shown in Fig. 7. In theory, stationary mountain waves will be attenuated into the mean flow at the *zero-wind level*, which is known as *critical level absorption* [*Booker and Bretherton*, 1967].

In winter (Fig. 7a), a critical level is present in the upper troposphere near z = 7 km south of 20°N. Consequently, the OGWD is absent in the middle atmosphere of lower latitudes (Figs. 2a and 4a). In mid-latitudes, there is no preexisting critical level. The most striking features are the two jets (with horizontal wind speed greater than 25 m s^{-1}) located in the upper troposphere-lower stratosphere and near the stratopause. The weak wind (less than 10 m s^{-1}) between the two jets provides a favorable condition for mountain wave breaking, because the waves can readily induce a critical level where $\overline{\mathbf{V}} + \mathbf{v}' = 0$. As such, the mid-lower-latitude OGWD mainly occurs above the upper-tropospheric jet. This also explains the occurrence of OGWD in the lowermost stratosphere of high latitudes, given the weak wind there. The breaking of mountain waves in the weak wind layer of lower stratosphere has been confirmed by lidar observations [*Ehard et al*., 2017]. In summer (Fig. 7b), there is a broad wind reversal spanning the Northern Hemisphere such that the OGWD generally vanishes in the upper stratosphere and lower mesosphere (Figs. 2c and 4c). However, weak OGWD is found near the stratopause of lower latitudes, located in small regions of southern Rocky Mountains, Arabian Peninsula and northern Africa (Fig. 3d). It is because the background wind shown is for 6-yr average. Mountain waves can reach the upper atmosphere in days without wind reversal. This finding agrees with *Sato et al*. [2009] in that the lower-latitude monsoon region is the most important window to the middle atmosphere in summer.

As revealed by the notable difference between OGWD_H and OGWD_V(e.g., Fig. 5), the horizontal propagation of mountain waves has a great influence on the mountain wave drag. In accordance with *Eckermann et al*. [2015] and X17, the horizontal propagation of mountain waves can reduce the local wave amplitude with height. Therefore, mountain waves in the X17 scheme are prone to break at higher altitudes than in the LM97 scheme. This is clearly shown in Fig. 8 which depicts the profiles of vertical displacement amplitude of the mountain waves in western Tibetan Plateau (82.5°E, 32.5°N) and northern Rocky Mountains (130°W, 62.5°N) respectively. The wave amplitude in the X17 scheme is obtained from the GBA solution, whereas in the LM97 scheme it is obtained according to the conservation of wave action. Readers are referred to X17 for more details. Mountain waves in western Tibetan Plateau basically break in the middle stratosphere between z = 20 km and 30 km where the wave amplitude exceeds the saturation wave amplitude (Fig. 8a). In contrast, the waves in the high latitude of northern Rocky Mountains saturate and break in the upper stratosphere and lower mesosphere above z = 35 km (Fig. 8b). Nonetheless, in both cases the wave amplitude in the X17 scheme is smaller than in the LM97 scheme, giving rise to higher breaking levels.

Klinker and Sardeshmukh [1992] have diagnosed the momentum budget for the ECMWF model in January 1987. Excessive mountain wave drag was found in the lower stratosphere (on the order of 1 m s^{-1} day^{-1}, see their Fig. 3b). This drag bias agrees very well with the difference found herein (about 10^{-5} m s^{-2}, i.e., 0.864 m s^{-1} day^{-1}, see Fig. 5a). It suggests that including the horizontal propagation of mountain waves in the parameterization of OGWD can help reduce the too large mountain wave drag in the lower stratosphere of climate models. Owing to the height decay of air density, mountain waves should ultimately break and deposit the wave momentum into the mean flow. The decrease of OGWD in the lower stratosphere implies that more gravity wave momentum will be transported to higher altitudes, which accounts for the notable increase of mountain wave drag in the upper stratosphere and lower mesosphere in the X17 scheme (Fig. 5). As mentioned in the introduction, *Long et al*. [2012] found significant temperature biases in the mesosphere of Met Office middle atmospheric analyses, which were ascribed to insufficient gravity wave forcing there. Here the results show that taking into account the horizontal propagation of mountain waves can potentially alleviate this model bias.

4 Summary

This study investigates the OGWD in the stratosphere and lower mesosphere of Northern Hemisphere during 2011-2016 using two different parameterization schemes. One is the scheme adopted in the ECMWF forecast model; the other is the scheme proposed in X17 that takes into account the horizontal propagation of mountain waves. The main purpose is to provide an insight into the impact of horizontal propagation on the OGWD, which is tacitly neglected in traditional OGWD parameterization schemes.

According to the 2.5° ERA-interim reanalysis and the 1-arc-minute ETOPO1 terrain data, two sets of OGWD are calculated offline respectively. In both cases, the OGWD experiences a notable seasonal variation induced by the seasonal cycle of the mean flow circulation. In winter, the mountain wave drag in mid-lower latitudes is mainly located in the weak wind layer of lower stratosphere between the two jets in the upper troposphere and lower mesosphere. By contrast, OGWD is observed in the whole stratosphere of mid-high latitudes, due to the weak background wind there. The mid-high-latitude OGWD shows an increasing trend with height, which is likely caused by the height decay of air density. The summertime OGWD is in general confined in the lower stratosphere, as the reversal of background wind forms a broad critical level spanning the Northern Hemisphere. Nevertheless, weak OGWD is still observed in the upper stratosphere and lower mesosphere of lower latitudes, suggesting that the summer monsoon region is an important window to the middle atmosphere. Comparison between the two sets of OGWD reveals that the mountain wave drag is suppressed (enhanced) in the lower stratosphere (mid-upper stratosphere and lower mesosphere) when the horizontal propagation of mountain waves is taken into account. This effect is more prominent in winter than in summer, with the drag in western Tibetan Plateau, Rocky Mountains, and Greenland greatly impacted.

The results suggest there is a need to incorporate the horizontal propagation of mountain waves in the parameterization of OGWD, which can potentially alleviate the commonly seen wind and temperature biases in climate models. For one thing, it can help reduce the excessive mountain wave drag in the lower stratosphere; for another, more mountain waves are allowed to propagate into the mesosphere, producing more gravity wave forcing there. In the present study, the impact of horizontal propagation of mountain waves is investigated offline using reanalysis dataset. In order to better understand this effect, the X17 scheme will be implemented in a global model which enables the interaction between mountain waves and the mean flow.

In the calculation of OGWD, the direction change of background wind with height is not considered, as mentioned in section 3.3. In fact, the *directional wind shear* is omitted in all existing OGWD parameterization schemes. Recently, there is an increasing interest in mountain waves generated in directionally sheared wind [e.g., *Eckermann et al*., 2007; *Teixeira and Miranda*, 2009; *Teixeria and Yu*, 2014; *Xu et al*., 2012, 2013, 2017a; *Guarino et al*., 2016], however. In this situation, there are an infinite number of critical levels corresponding to different wave components; in consequence, mountain waves are continuously attenuated into the mean flow during their upward propagation [*Broad*, 1995]. If the background wind rotates substantially in the lower atmosphere, mountain waves will primarily deposit the wave momentum in the troposphere and affect the tropospheric circulation rather than the general circulation in the middle atmosphere. More importantly, the *selective critical level* absorption of mountain waves produces a body force *perpendicular* to the background wind, rather than parallel to it [*Broad*, 1995; *Xu et al.*, 2012]. *Martin and Lott* [2007] examined the synoptic response to the selective critical level absorption of mountain waves using a heuristic model. Their results showed that potential vorticity (PV) anomalies can be generated in the midtroposphere, accompanied with cyclonic (anticyclonic) circulation for backing (veering) wind. The impact of directional wind shear on the momentum transport of mountain waves will be evaluated in an upcoming study.

Acknowledgments. This study is supported by National Fundamental Research 973 Program of China (2015CB452801 and 2013CB430103) and National Science Foundation of China (Grant 41505046). The ETOPO1 data is available at https://www.ngdc.noaa.gov/mgg/global/global.html; the ERA-interim reanalysis can be downloaded at https://www.ecmwf.int/en/research/climate-reanalysis/era-interim.

References

Alexander, M. J., and H. Teitelbaum (2011), Three-dimensional properties of Andes mountain waves observed by satellite: A case study, J. Geophys. Res., 116, D23110, doi: 10.1029/2011JD016151.

Alexander, M. J., S. D. Eckermann, D. Broutman, and J. Ma (2009), Momentum flux estimates for South Georgia Island mountain waves in the stratosphere observed via satellite, Geophys. Res. Lett., 36, L12816, doi: 10.1029/2009GL038587.

Amante, C. and B.W. Eakins (2009), ETOPO1 1 Arc-Minute Global Relief Model: Procedures, Data Sources and Analysis. NOAA Technical Memorandum NESDIS NGDC-24, National Geophysical Data Center, NOAA, doi: 10.7289/V5C8276M.

Booker, J. R., and F. P. Bretherton (1967), The critical layer for internal gravity waves in a shear flow, J. Fluid Mech., 27, 513–539, doi: https://doi.org/10.1017/S0022112067000515.

Broad, A. S. (1995), Linear theory of momentum fluxes in 3-D flows with turning of the mean wind with height, Q. J. R. Meteorol. Soc., 121, 1891–1902, doi: 10.1002/qj.49712152806

Broutman, D., S. D. Eckermann, H. Knight, and J. Ma (2017), A stationary phase solution for mountain waves with application to mesospheric mountain waves generated by Auckland Island, J. Geophys. Res. Atmos., 122, 699–711, doi:10.1002/2016JD025699.

Calvo, N., R. R. Garcia, and D. E. Kinnison (2017), Revisiting Southern Hemisphere polar stratospheric temperature trends in WACCM: The role of dynamical forcing, Geophys. Res. Lett., 44, 3402–3410, doi:10.1002/2017GL072792.

Choi, H.-J., and S.-Y. Hong (2015), An updated subgrid orographic parameterization for global atmospheric forecast models, J. Geophys. Res. Atmos., 120, 12,445–12,457, doi: 10.1002/2015JD024230.

Dee, D. P., and Coauthors, 2011: The ERA-Interim reanalysis: Configuration and performance of the data assimilation system. Quart. J. Roy. Meteor. Soc., 137, 553–597, doi: 10.1002/qj.828.

Eckermann, S. D., J. Ma, and D. Broutman (2015), Effects of horizontal geometrical spreading on the parameterization of orographic gravity wave drag. Part I: Numerical transform solutions, J. Atmos. Sci., 72, 2330–2347, doi: 10.1175/JAS-D-14-0147.1.

Eckermann, S. D., J. Ma, D. L. Wu, and D. Broutman (2007), A three-dimensional mountain wave imaged in satellite radiance throughout the stratosphere: Evidence of the effects of directional wind shear, Q. J. R. Meteorol. Soc., 133, 1959–1975, doi: 10.1002/qj.187.

Ehard, B., and Coauthors (2017), Vertical propagation of large-amplitude mountain waves in the vicinity of the polar night jet, J. Geophys. Res. Atmos., 122, 1423–1436, doi: 10.1002/2016JD025621.

Fritts, D. C., and M. J. Alexander (2003), Gravity wave dynamics and effects in the middle atmosphere, Rev. Geophys., 41, 1003, doi: 10.1029/2001RG000106.

Garcia, R. R., A. K. Smith, D. E. Kinnison, A. de la Cámara, and D. J. Murphy (2017), Modification of the gravity wave parameterization in the Whole Atmosphere Community Climate Model: Motivation and results, J. Atmos. Sci., 74, 275–291, doi: 10.1175/JAS-D-16-0104.1.

Guarino, M. V., M. A. C. Teixeira, and M. H. P. Ambaum (2016), Turbulence generation by mountain wave breaking in flows with directional wind shear, Quart. J. Roy. Meteor. Soc., 142, 2715–2726, doi: 10.1002/qj.2862.

Haynes, P. H., C. J. Marks, M. E. McIntyre, T. G. Shepherd, and K. P. Shine (1991), On the “downward control” of extratropical diabatic circulations by eddy-induced mean zonal forces, J. Atmos. Sci., 48, 651–678, doi: 10.1175/1520-0469(1991)048<0651:OTCOED>2.0.CO;2.

Holton, J. R. (1983), The influence of gravity wave breaking on the general circulation of the middle atmosphere, J. Atmos. Sci., 40, 2497–2507, doi: 10.1175/1520-0469(1983)040<2497:TIOGWB>2.0.CO;2.

Kim, Y. J. (2007), Balance of drag between the middle and lower atmospheres in a global atmospheric forecast model, J. Geophys. Res. Atmos., 112, D13104, doi: 10.1029/2007JD008647.

Kim, Y. J., and J. D. Doyle (2005), Extension of an orographic-drag parameterization scheme to incorporate orographic anisotropy and flow blocking, Q. J. R. Meteorol. Soc., 131, 1893–1921, doi: 10.1256/qj.04.160.

Klinker, E., and P. D. Sardeshmukh (1992), The diagnosis of mechanical dissipation in the atmosphere from large-scale balance requirements, J. Atmos. Sci., 49, 608–627, doi: 10.1175/1520-0469(1992)049<0608:TDOMDI>2.0.CO;2.

Long D. J., D. R. Jackson, J. Thuburn, and C. Mathison (2012), Validation of Met Office upper stratospheric and mesospheric analyses, Q. J. R. Meteorol. Soc., 139, 1214–1228, doi: 10.1002/qj.2031.

Lott, F., and M. Miller (1997), A new sub-grid orographic drag parameterization: Its formulation and testing, Quart. J. Roy. Meteor. Soc., 123, 101–127, doi: 10.1002/qj.49712353704.

Martin, A., and F. Lott (2007), Synoptic responses to mountain gravity waves encountering directional critical levels, J. Atmos. Sci., 64, 828–848, doi: 10.1175/JAS3873.1.

Miranda, P. M. A., and I. N. James (1992), Non-linear three dimensional effects on gravity-wave drag: Splitting flow and breaking waves. Quart. J. Roy. Meteor. Soc., 118, 1057–1081, doi: 10.1002/qj.49711850803.

McLandress, C., and T. G. Shepherd (2009), Simulated anthropogenic changes in the Brewer-Dobson circulation, including its extension to high latitudes, J. Clim., 22, 1516–1540, doi:10.1175/2008JCLI2679.1.

McLandress, C., T. G. Shepherd, S. Polavaparu, and S. R. Beagley (2012), Is missing orographic gravity wave drag near 60°S the cause of the stratospheric zonal wind biases in chemistry–climate models? J. Atmos. Sci., 69, 802–818, doi: 10.1175/JAS-D-11-0159.1.

Palmer, T. N., G. J. Shutts, and R. Swinbank (1986), Alleviation of systematic westerly bias in general circulation and numerical weather prediction models through an orographic gravity wave drag parameterization. Quart. J. Roy. Meteor. Soc., 112, 1001–1039, doi:10.1002/qj.49711247406.

Pulido, M., and C. Rodas (2011), A higher-order ray approximation applied to orographic waves: Gaussian beam approximation, J. Atmos. Sci., 68, 46–60, doi: 10.1175/2010JAS3468.1.

Polvani, L. M., D. W. Waugh, G. J. P. Correa, and S.-W. Son (2011), Stratospheric ozone depletion: The main driver of twentieth-century atmospheric circulation change in the Southern Hemisphere, J. Clim., 24, 795–812, doi: 10.1175/2010JCLI3772.1.

Sandu, I., P. Bechtold, A. Beljaars, A. Bozzo, F. Pithan, T. G. Shepherd, and A. Zadra (2016), Impacts of parameterized orographic drag on the Northern Hemisphere winter circulation, J. Adv. Model. Earth Syst., 8, 196–211, doi:10.1002/2015MS000564.

Sato, K., S. Watanabe, Y. Kawatani, Y. Tomikawa, K. Miyazaki, and M. Takahashi (2009), On the origins of gravity waves in the mesosphere, Geophys. Res. Lett., 36, L19801, doi:10.1029/2009GL039908.

Scinocca, J. F., and N. A. McFarlane (2000), The parametrization of drag induced by stratified flow over anisotropic orography, Quart. J. Roy. Meteor. Soc., 126, 2353–2393, doi: 10.1002/qj.49712656802.

Smith, R. B. (1980), Linear theory of stratified hydrostatic flow past an isolated mountain. Tellus, 32, 348–364, doi: 10.1175/1520-0469(1988)045<3889:LTOSFP>2.0.CO;2.

Teixeira, M. A. C., and P. M. A. Miranda (2009), On the momentum fluxes associated with mountain waves in directionally sheared flows. J. Atmos. Sci., 66, 3419–3433, doi: 10.1175/2009JAS3065.1.

Teixeira, M. A. C., and C. L. Yu (2014), The gravity wave momentum flux in hydrostatic flow with directional shear over elliptical mountains. European Journal of Mechanics-B/Fluids, 47, 16-31, doi: 10.1016/j.euromechflu.2014.02.004.

Teixeira, M. A. C., P. M. A. Miranda, and M. A. Valente (2004), The effect of wind shear and curvature on the gravity wave drag produced by a ridge. J. Atmos. Sci., 61, 2638–2643, doi:10.1175/JAS3282.1.

Xu, X., Y. Wang, and M. Xue (2012), Momentum flux and flux divergence of gravity waves in directional shear flows over three-dimensional mountains, J. Atmos. Sci., 69, 3733−3744, doi: 10.1175/JAS-D-12-044.1.

Xu, X., M. Xue, and Y. Wang (2013), Gravity wave momentum flux in directional shear flows over three-dimensional mountains: Linear and nonlinear numerical solutions as compared to linear analytical solutions, J. Geophys. Res. Atmos., 118, 7670−7681, doi: 10.1002/jgrd.50471.

Xu, X., J. J. Song, Y. Wang, and M. Xue (2017), Quantifying the Effect of Horizontal Propagation of Three-Dimensional Mountain Waves on the Wave Momentum Flux Using Gaussian Beam Approximation, J. Atmos. Sci., 74, 1783–1798, doi: 10.1175/JAS-D-16-0275.1.

List of Figures

Figure 6. Geographical distribution of OGWD_D (unit: 10^{-4} m s^{-2}) in the layers of (a) z = 16~18 km, (b) z = 20~22 km, and (c) z = 40~50 km in winter. (d)-(f) are similar to (a)-(c) but for OGWD_D in the layers of (d) z = 14~16 km (e) z = 18~20 km and (f) z = 40~50 km in summer.

Figure 7. Zonal-mean background wind (unit: m s^{-1}) between the upper troposphere and lower mesosphere of Northern Hemisphere averaged during 2011-2016 in (a) winter and (b) summer.

Figure 8. Profiles of vertical displacement amplitude of the mountain waves (unit: m) in the western Tibetan Plateau (82.5°E, 32.5°N) and northern Rocky Mountains (130°W, 62.5°N) averaged in December 2013. Solid line is the saturation wave amplitude, with dashed and dotted lines representing the wave amplitudes obtained in the LM97 and X17 schemes respectively.

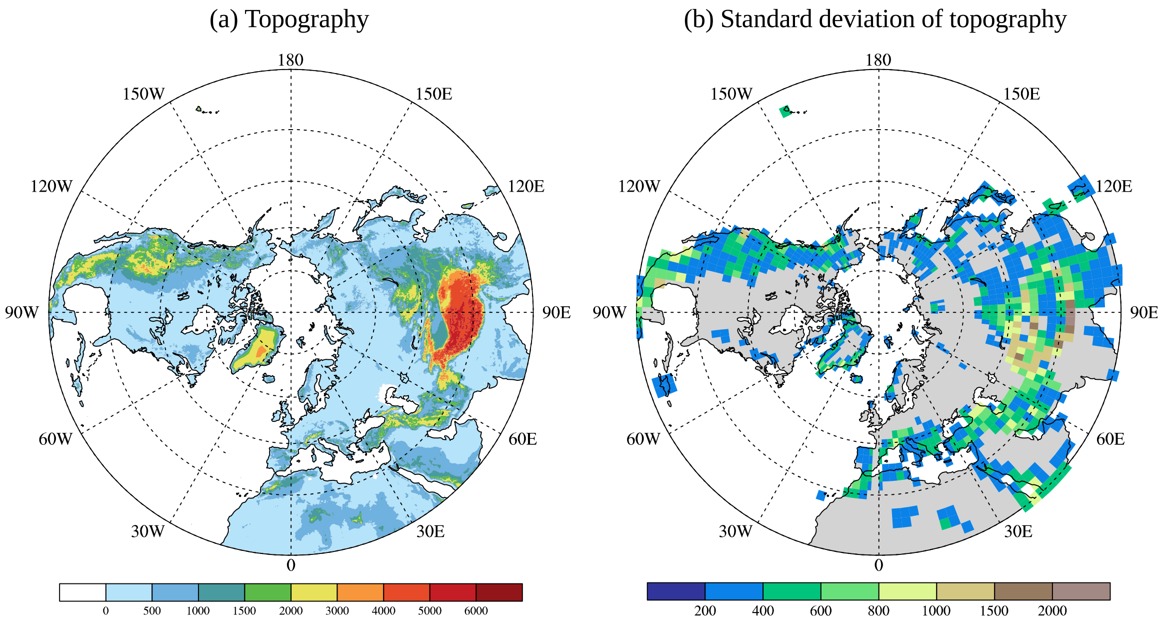

Figure 1. (a) 1-arc-min topography (unit: m) and (b) standard deviation (unit: m) of topography within the 2.5° ECMWF ERA-interim reanalysis grids in the Northern Hemisphere. The latitudes are shown every 15 degrees starting from 15°N.

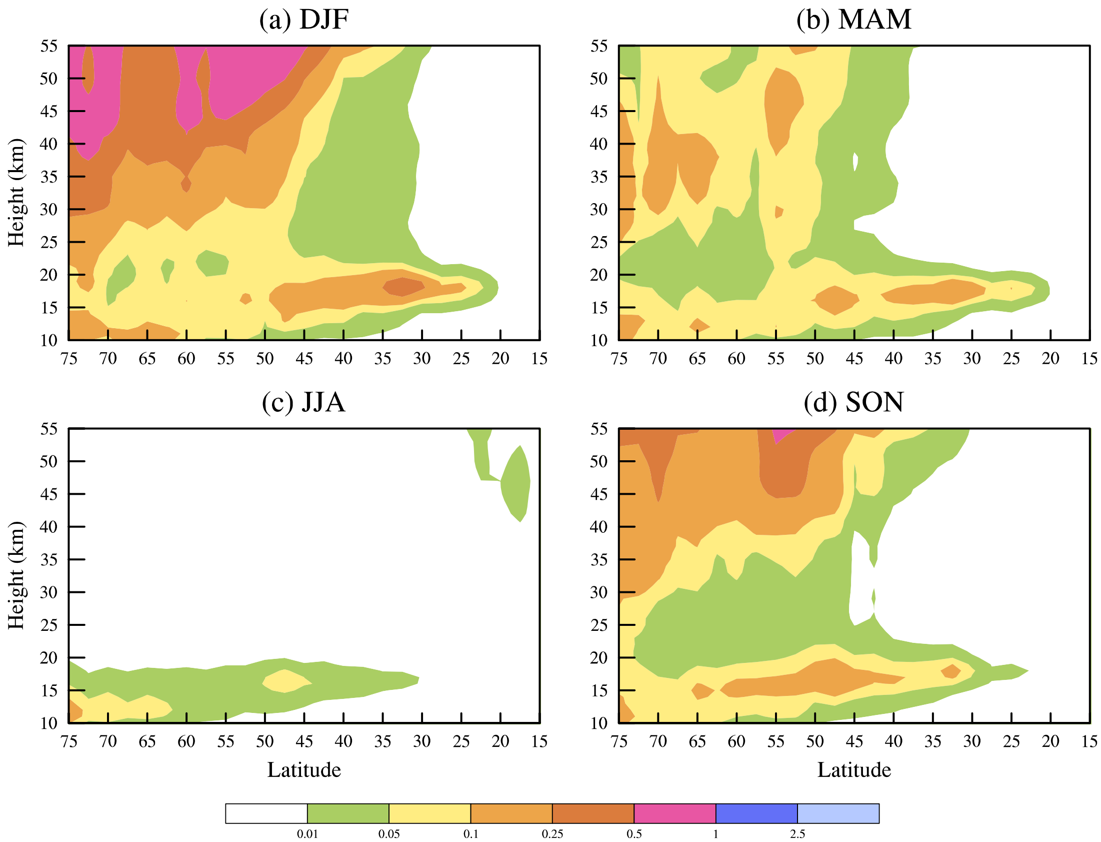

Figure 2. Zonal-mean OGWD_V (unit: 10^{-4} m s^{-2}) in the stratosphere and lower mesosphere of Northern Hemisphere averaged during 2011-2016. (a) Winter, (b) spring, (c) summer, and (d) autumn.

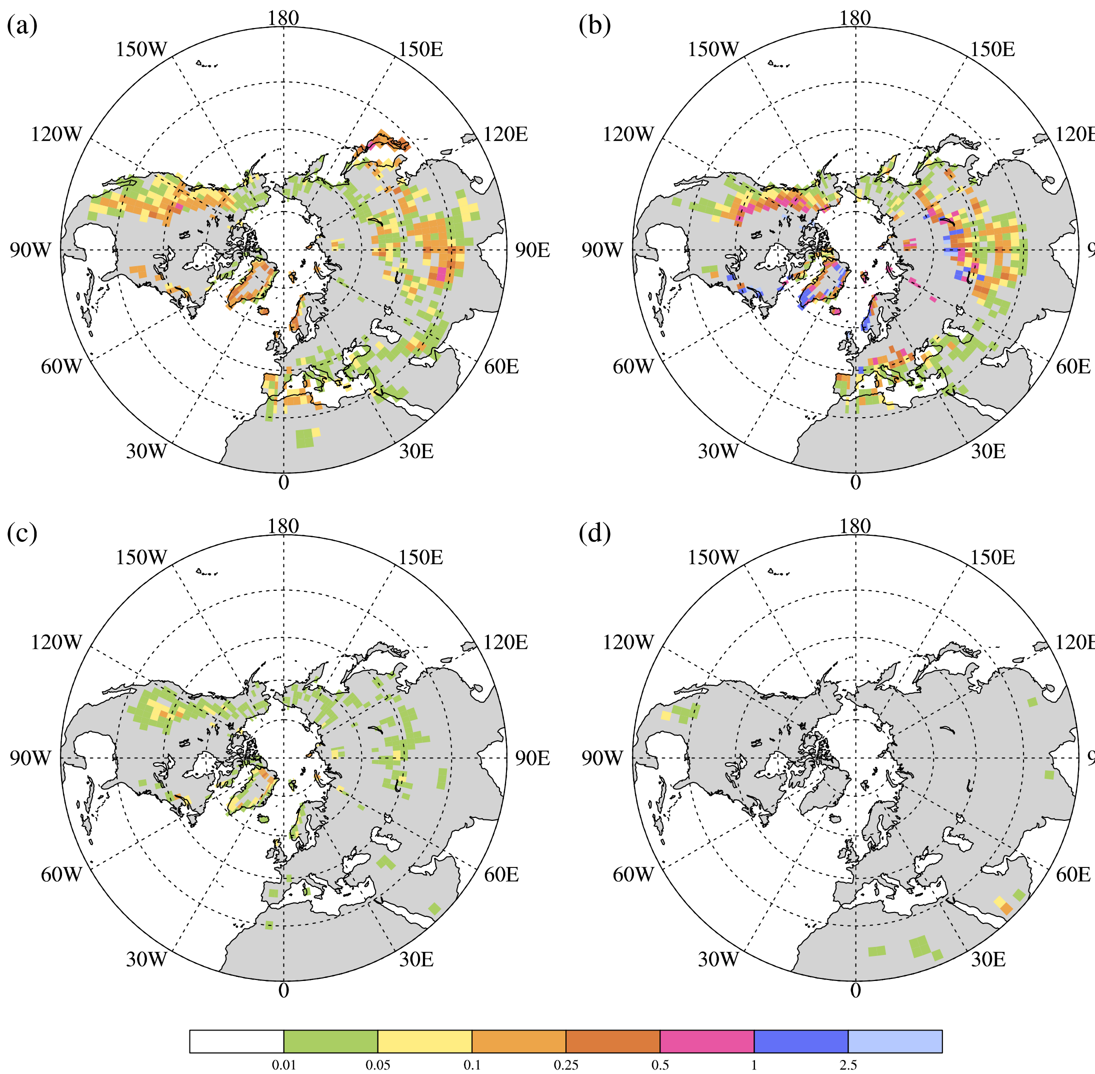

Figure 3. Geographical distribution of OGWD_V (unit: 10^{-4} m s^{-2}) in the (a) (c) mid-lower stratosphere between z = 10 km and 25 km, and (b) (d) upper stratosphere and lower mesosphere between z = 40 km and 55 km averaged during 2011-2016. (a) and (b) are in winter while (c) and (d) are in summer. The latitudes are shown every 15 degrees starting from 15°N.

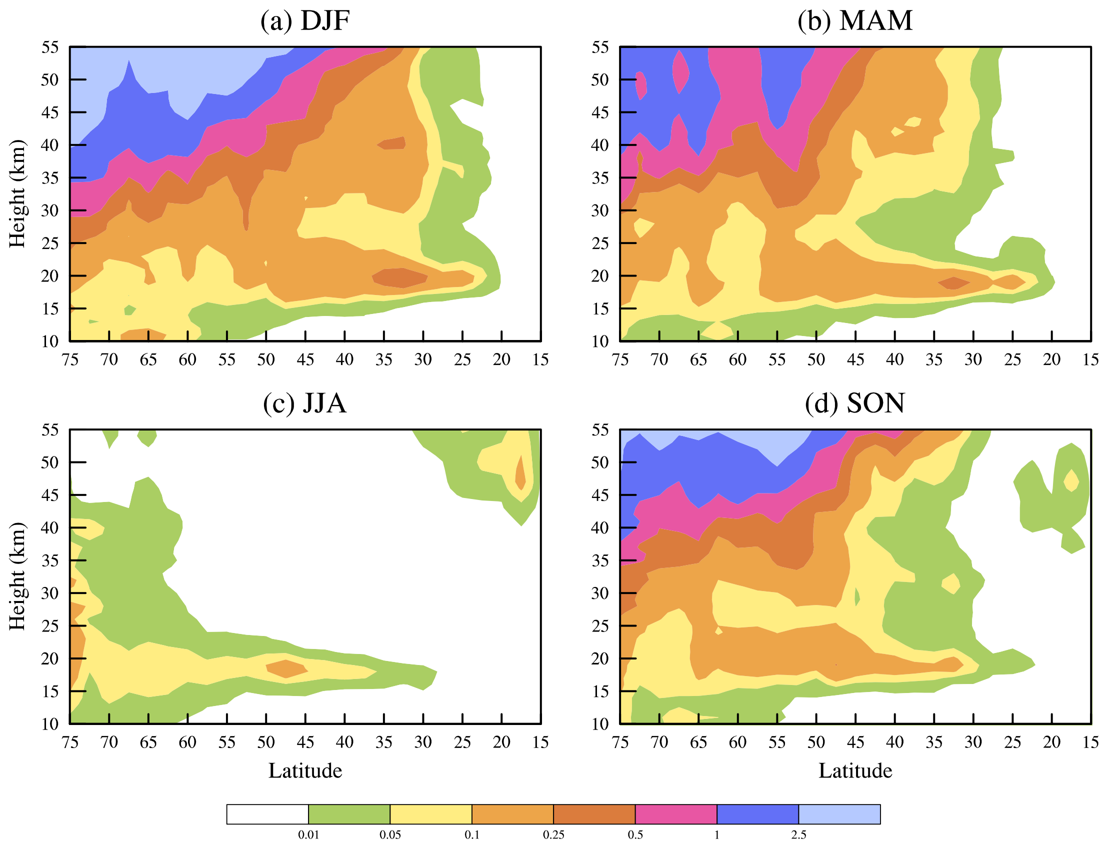

Figure 4. Same as Fig. 2 but for OGWD_H (unit: 10^{-4} m s^{-2}) in the stratosphere and lower mesosphere of Northern Hemisphere averaged during 2011-2016. (a) Winter, (b) spring, (c) summer, and (d) autumn.

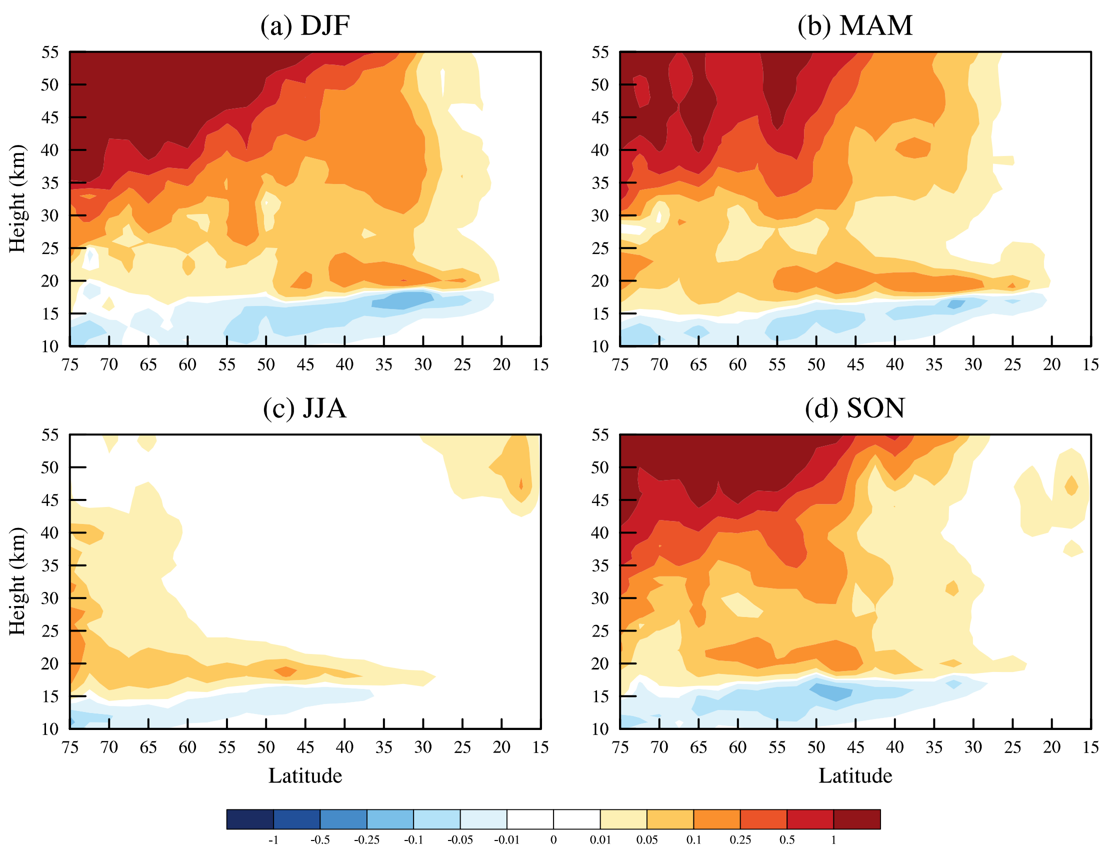

Figure 5. Same as Fig. 2 but for OGWD_D (unit: 10^{-4} m s^{-2}) in the stratosphere and lower mesosphere of Northern Hemisphere averaged during 2011-2016. (a) Winter, (b) spring, (c) summer, and (d) autumn.

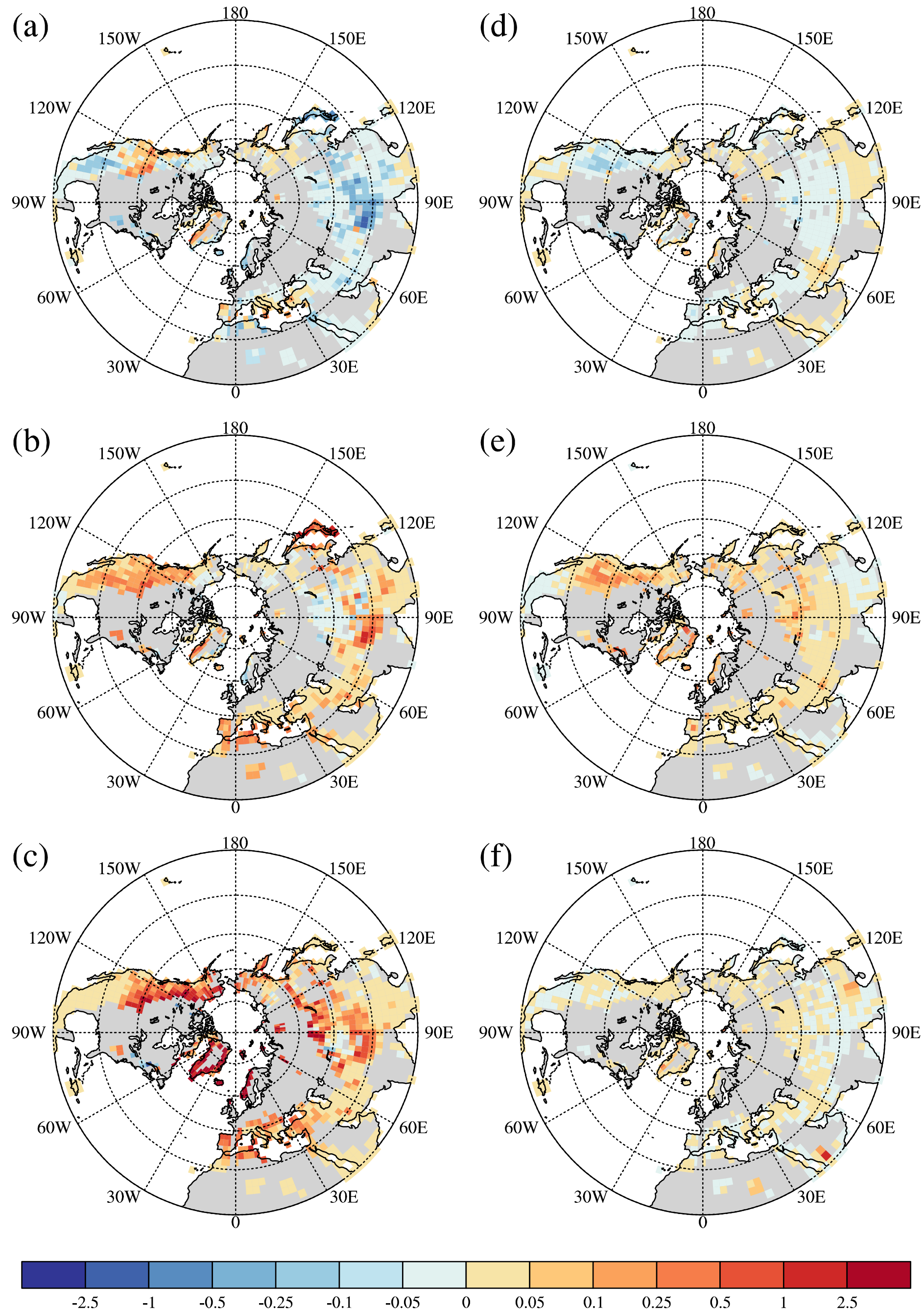

Figure 6. Geographical distribution of OGWD_D (unit: 10^{-4} m s^{-2}) in the layers of (a) z = 16~18 km, (b) z = 20~22 km, and (c) z = 40~50 km in winter. (d)-(f) are similar to (a)-(c) but for OGWD_D in the layers of (d) z = 14~16 km (e) z = 18~20 km and (f) z = 40~50 km in summer. The latitudes are shown every 15 degrees starting from 15°N.

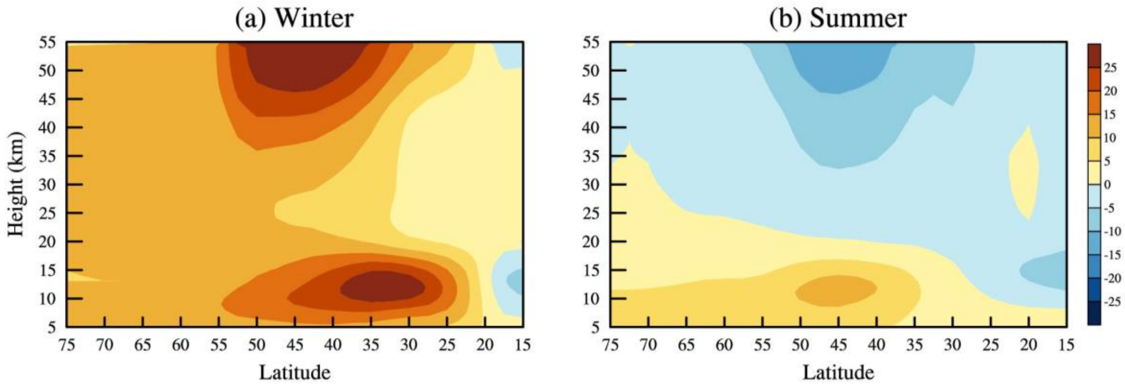

Figure 7. Zonal-mean background wind (unit: m s^{-1}) between the upper troposphere and lower mesosphere of Northern Hemisphere averaged during 2011-2016 in (a) winter and (b) summer.

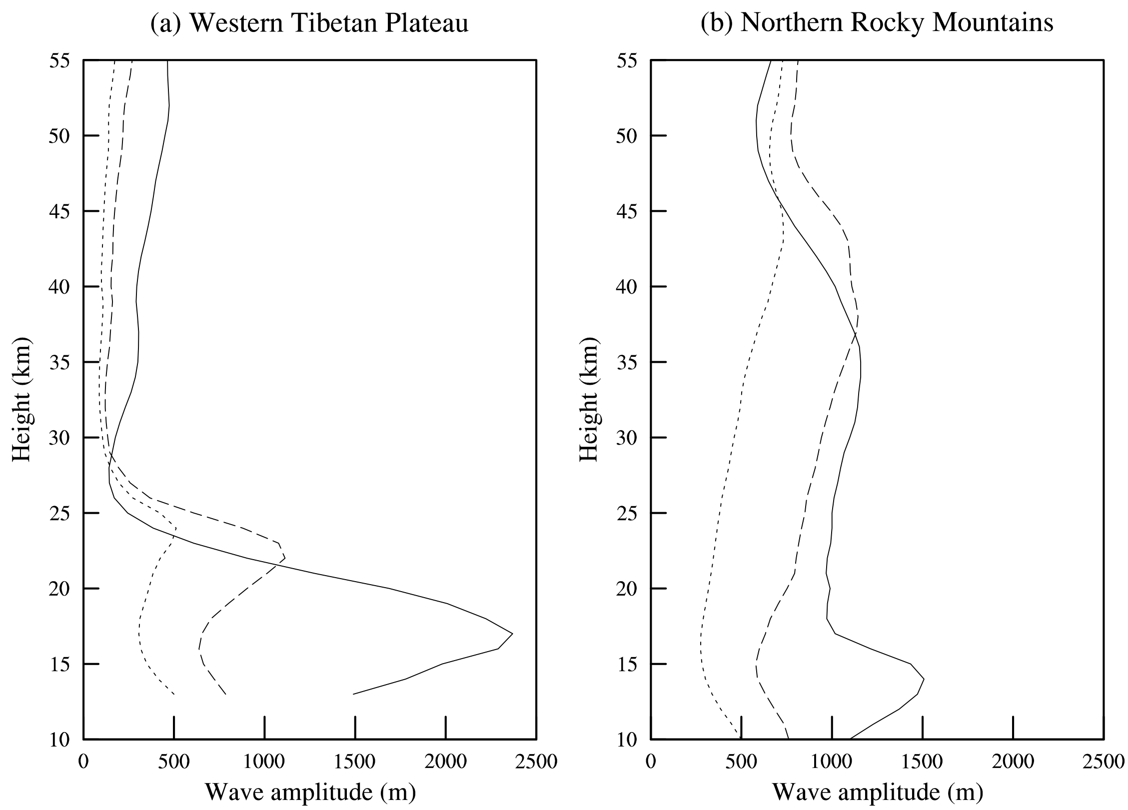

Figure 8. Profiles of vertical displacement amplitude of the mountain waves (unit: m) in the western Tibetan Plateau (82.5°E, 32.5°N) and northern Rocky Mountains (130°W, 62.5°N) averaged in December 2013. Solid line is the saturation wave amplitude, with dashed and dotted lines representing the wave amplitudes obtained in the LM97 and X17 schemes respectively.